Available online at www.sciencedirect.com
SCIENCE DIRECT®
Journal of Sound and Vibration 273 (2004) 805–836
JOURNAL OF SOUND AND VIBRATION
www.elsevier.com/locate/jsvi

On the stability of rotating blade arrays

G. Genta*

Politecnico di Torino, Department of Mechanics, Corso Duca degli Abruzzi 24, Torino 10039, Italy

Received 23 January 2003; accepted 8 May 2003

Abstract

A mathematical model consisting of an array of rotating pendulums was built to study the stability of an array of rotating blades and the dynamic interaction between the blades and the rotor. This model can be solved in closed form, yielding some general results regarding the stability of the system, particularly for the effects of the blade–rotor interaction and of blade damping. The closed form solution so obtained is then checked against a more realistic finite element method (FEM) model in which the blades are modelled as beams. As a result, the possibility that the disc–blades interaction gives way to instability even in the case of undamped systems, which has been known for many years, is confirmed for the case of in-plane oscillations of 'long' blades. The damping associated to bladed arrays, although rotating, is shown not to have an unstabilizing effect but, on the contrary, to help in counteracting the above-mentioned instability.

1. Introduction

The instability of propellers due to the interaction between the dynamics of the blades and that of the engine suspension is a well-known phenomenon [1,2]. This kind of instability may also occur in rotating blades arrays, like those present in turbomachinery. Other instability mechanisms may well be present: the role of damping in rotordynamics has been well known for more than half a century [2–5]. All damping which can be associated to the non-rotating parts of the machine has the usual stabilizing role as in structural dynamics, but damping of rotating elements can trigger instability in the supercritical range. What actually happens is that rotating damping couples rotational motion and vibration, causing energy to be transferred from the former to the latter. This phenomenon is general, occurring every time energy dissipation takes place in a rotating system: eddy current dampers in which energy is dissipated in the rotor can

*Fax: +39-011-564-6999.
E-mail address: giancarlo.genta@polito.it (G. Genta).
URL: http://www.giancarlogenta.it.

0022-460X/$ - see front matter © 2003 Elsevier Ltd. All rights reserved.
doi:10.1016/S0022-460X(03)00784-3

cause instability in the supercritical regime, while if energy is dissipated into the stator do not. The same occurs in celestial dynamics when a satellite induces tides in a spinning planet and causes the orbit of the Moon to grow in time and the rotation of the Earth about its axis to slow down. Another instance is oil whip, caused by the viscosity of an oil film rotating at a speed about half of the rotor speed [6].

Rotor damping is not the only cause of instability, and there are cases in which even an undamped rotating system can become unstable. In the aforementioned instability of propellers as well as in that of rotors partially filled with fluid, instability is linked with a wave propagating in the rotor in a forward direction with respect to a non-rotating frame while it propagates in a backward direction in a rotor-fixed frame [2,7].

Some doubts were cast on the unstabilizing effect of rotating damping in the case of bladed discs. This is in no way just an academic matter. To prevent blade vibration, dampers can be located in the disc: there is no doubt that these devices stabilize the motion of the rotor in subcritical condition, but will they have an unstabilizing effect in the supercritical range?

The study of the dynamics of a bladed disc is quite complex and must be performed using numerical models. To obtain a closed form solution, suitable for a stability analysis, it is possible to resort to simplified models, like the ones used in the past for instance in Refs. [1,2], where the blades are substituted by rotating pendulums, but generalizing them to the case of an indeterminate number n of blades.

2. Dynamics of a row of rotating pendulums

2.1. Model definition

Consider a rigid rotor, with mass, polar and transversal moments of inertia m_d, J_p and J_t (symbols are listed in Appendix B), driven at a constant speed Ω on damped elastic isotropic supports with stiffness matrix $\mathbf{K}$ and damping matrix $\mathbf{C}$. At the periphery of the rigid body, in a plane perpendicular to the rotation axis containing the centre of mass of the system, there is a row of n (with $n \geqslant 3$) identical rotating spherical pendulums, each one with a length l and a mass m. Each pendulum is provided with a restoring spring, with rotational stiffness k_p, and a damper with damping coefficient $l^2 c_p$. A further number n of viscous dampers with damping coefficient c_q are located between the bobs of two subsequent pendulums. The latter have been introduced to simulate the damping acting between the blades (Fig. 1).

The system has a total of $(6 + 2n)$ degrees of freedom. The rigid rotor has six-degrees-of-freedom; using a standard approach it is possible to take as generalized co-ordinates the lateral displacements X and Y and the axial displacement Z of the centre of the rotor (point C in [5, Fig. 4.15]), the flexural rotations ϕ_X and ϕ_y and the torsional rotation ϕ_z defined with respect to the fixed (inertial) frame XYZ and the rotating (rotor-fixed) frame xyz defined in Ref. [5, Section 4.4.1]. Since the disc is assumed to be perfectly balanced, the geometric centre of the shaft C coincides with the centre of mass of the whole system, considered with the pendulums locked in their radial position.

The generalized co-ordinates for the pendulums are n in-plane rotation angles ϕ_i $(i = 1, \ldots, n)$ and n out-of-plane rotation angles γ_i.

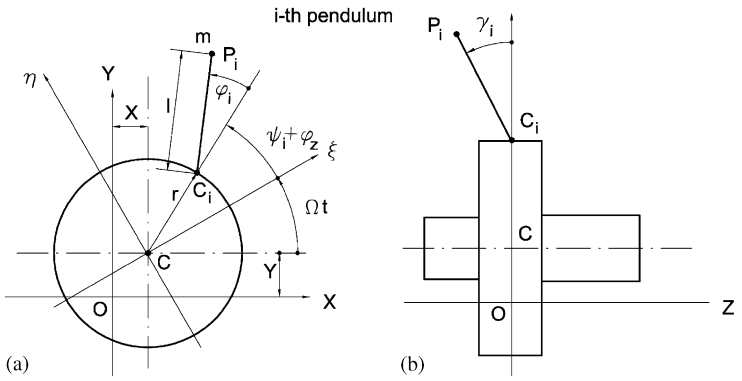

Fig. 1. Sketch of the position of the ith pendulum of the array: (a) projection in XY plane; (b) side view.

The suspension system is assumed to allow uncoupling between axial, torsional and lateral (flexural) behaviour and hence the axial, torsional and lateral stiffness and damping matrices can be considered as independent from each other. Moreover, axial symmetry allows elastic uncoupling between the lateral behaviour in xz and yz planes. The suspension system is considered as non-rotating; this is realistic for the axial and lateral behaviour (the stiffness and damping are attributed to the stator or the bearings), while for the torsional behaviour it would be better to associate the stiffness and the damping to the (rotating) drive system. However this point has little importance and will be dealt with later.

2.2. Uncoupled dynamics

Pendulums: If the supports of the disc are rigid and the pendulums do not have any restoring spring or damper, the usual results for rotating pendulums apply. By linearizing the equations of motion and neglecting gravitational acceleration, as usual with rotating pendulums, the natural frequency of the pendulums are [5]

$$\omega_{ip} = \Omega\sqrt{\frac{r}{l}} \quad \text{(in-plane dynamics)}, \tag{1}$$

$$\omega_{op} = \Omega\sqrt{1+\frac{r}{l}} \quad \text{(out-of-plane dynamics)} \tag{2}$$

Rigid rotor: If the pendulums are locked in their radial position, the system behaves as a single rigid body with the following inertial properties:

$$m_T = m_d + nm, \quad J_{t_T} = J_t + \frac{nm(r+l)^2}{2}, \quad J_{p_T} = J_p + nm(r+l)^2, \tag{3}$$

where m_T is the total mass of the system.

By resorting to the usual small displacements and rotations assumption, the axial, torsional and lateral behaviour of the rigid rotor are uncoupled. The axial and torsional natural frequencies of

the undamped system do not depend on the speed and are

$$\omega_{ax} = \sqrt{\frac{k_a}{m_T}}, \quad \omega_{tors} = \sqrt{\frac{k_t}{J_{p_T}}}. \tag{4}$$

The lateral natural frequencies can be computed using Eq. (4.73) in [5]

$$\omega_l^4 - \omega_l^3 \Omega \frac{J_{p_T}}{J_{t_T}} - \omega_l^2 \left(\frac{k_{11}}{m} + \frac{k_{22}}{J_{t_T}} \right) + \omega_l \Omega \frac{k_{11} J_{p_T}}{m J_{t_T}} + \frac{k_{11} k_{22} - k_{12}^2}{m J_{t_T}} = 0, \tag{5}$$

where k_{ij} are the elements of the stiffness matrix related to the lateral behaviour in xz plane.

Note that if $k_{12} = 0$ the lateral behaviour uncouples into a translational (cylindrical whirling) behaviour, whose natural frequency is

$$\omega_{l1} = \sqrt{\frac{k_{11}}{m_T}} \tag{6}$$

and is not affected by the spin speed (Jeffcott rotor model), and a rotational (conical whirling) behaviour, whose natural frequency is a function of the speed

$$\omega_{l2} = \frac{J_{p_T} \Omega \pm \sqrt{J_{p_T}^2 \Omega^2 + 4 J_{t_T} k_{22}}}{2 J_{t_T}}. \tag{7}$$

2.3. Coupled dynamics: equations of motion

To study the coupled dynamics the whole system with $(6 + 2n)$ degrees-of-freedom must be dealt with. The derivation of the Lagrangian and the Rayleigh dissipation function is quite intricate and is performed in Appendix A.

By performing the relevant derivatives of the kinetic and potential energy, and linearizing the results (remembering that ϕ_z and ϕ_i are small angles, while Ωt and ψ_i are not), the following linear equations of motion can be obtained:

- First equation (translation along X-axis)

$$\begin{aligned} m_T \ddot{X} - m \sum_{i=1}^{n} \{ & [l(\ddot{\phi}_i - \Omega^2 \phi_i) + \ddot{\phi}_z (r + l)] \sin(\theta_i) \\ & + [(\Omega^2 + 2\Omega \dot{\phi}_z)(r + l) + 2\Omega l \dot{\phi}_i] \cos(\theta_i) \} \\ & + c_{11} \dot{X} + c_{12} \dot{\phi}_y + k_{11} X + k_{12} \phi_y = 0. \end{aligned} \tag{8}$$

By remembering some trigonometrical identities and noting that

$$\sum_{i=1}^{n} \sin(\theta_i) = \sum_{i=1}^{n} \cos(\theta_i) = 0 \tag{9}$$

it is possible to write the first equation in the form

$$m_T\ddot{X} + ml\sum_{i=1}^{n}[(-\ddot{\phi}_i + \Omega^2\phi_i)\cos(\psi_i) + 2\Omega\dot{\phi}_i\sin(\psi_i)]\sin(\Omega t) + ml\sum_{i=1}^{n}[(-\ddot{\phi}_i + \Omega^2\phi_i)\sin(\psi_i) - 2\Omega\dot{\phi}_i\cos(\psi_i)]\cos(\Omega t) + c_{11}\dot{X} + c_{12}\dot{\phi}_y + k_{11}X + k_{12}\phi_y = 0. \quad (10)$$

- Second equation (translation along Y-axis)
  Operating in the same way, the second equation becomes

$$m_T\ddot{Y} + ml\sum_{i=1}^{n}[(\ddot{\phi}_i - \Omega^2\phi_i)\cos(\psi_i) - 2\Omega\dot{\phi}_i\sin(\psi_i)]\cos(\Omega t) + ml\sum_{i=1}^{n}[-(\ddot{\phi}_i - \Omega^2\phi_i)\sin(\psi_i) - 2\Omega\dot{\phi}_i\cos(\psi_i)]\sin(\Omega t) + c_{11}\dot{Y} - c_{12}\dot{\phi}_X + k_{11}Y - k_{12}\phi_X = 0. \quad (11)$$

- Third equation (translation along Z-axis)

$$m_T\ddot{Z} + ml\sum_{i=1}^{n}[\ddot{\gamma}_i + (l+r)(\ddot{\phi}_X + 2\dot{\phi}_y\Omega - \phi_X\Omega^2)\sin(\theta) + (l+r)(-\ddot{\phi}_y + 2\dot{\phi}_X\Omega + \phi_y\Omega^2)\cos(\theta)] + c_a\dot{Z} + k_aZ = 0, \quad (12)$$

  i.e.,

$$m_T\ddot{Z} + ml\sum_{i=1}^{n}\ddot{\gamma}_i + c_a\dot{Z} + k_aZ = 0. \quad (13)$$

- Fourth equation (rotation ϕ_y about y-axis)

$$\ddot{\phi}_yJ_t - \Omega\dot{\phi}_XJ_p + m(l+r)\sum_{i=1}^{n}\{-(\ddot{Z} + \gamma_il\Omega^2 + \ddot{\gamma}_il)\cos(\theta_i) + (l+r)(\ddot{\phi}_y - 2\Omega\dot{\phi}_X)\cos^2(\theta_i) - (l+r)(\ddot{\phi}_X + 2\Omega\dot{\phi}_y) \times \cos(\theta_i)\sin(\theta_i)\} + c_{11}\dot{\phi}_y + c_{12}\dot{X} + k_{11}\phi_y + k_{12}X = 0. \quad (14)$$

  By noting that

$$\sum_{i=1}^{n}\sin^2(\theta_i) = \sum_{i=1}^{n}\cos^2(\theta_i) = \frac{n}{2}, \quad \sum_{i=1}^{n}\sin(\theta_i)\cos(\theta_i) = 0 \quad (15)$$

the fourth equation becomes

$$\ddot{\phi}_y J_{t_T} - \Omega\dot{\phi}_X J_{p_T} - ml(r+l)\sum_{i=1}^{n}[\ddot{\gamma}_i + \Omega_i^2\gamma_i]\cos(\theta_i) + c_{11}\dot{\phi}_y + c_{12}\dot{X} + k_{11}\phi_y + k_{12}X = 0, \tag{16}$$

i.e.,

$$\ddot{\phi}_y J_{t_T} - \Omega\dot{\phi}_X J_{p_T} - ml(r+l)\cos(\Omega t)\sum_{i=1}^{n}[\ddot{\gamma}_i + \Omega^2\gamma_i]\cos(\psi_i) + ml(r+l)\sin(\Omega t)\sum_{i=1}^{n}[\ddot{\gamma}_i + \Omega^2\gamma_i]\sin(\psi_i) + c_{11}\dot{\phi}_y + c_{12}\dot{X} + k_{11}\phi_y + k_{12}X = 0. \tag{17}$$

- Fifth equation (rotation ϕ_X about X-axis)
  Operating in the same way, the fifth equation becomes

$$\ddot{\phi}_X J_{t_T} + \Omega\dot{\phi}_y J_{p_T} + ml(r+l)\sin(\Omega t)\sum_{i=1}^{n}[\ddot{\gamma}_i + \Omega^2\gamma_i]\cos(\psi_i) + ml(r+l)\cos(\Omega t)\sum_{i=1}^{n}[\ddot{\gamma}_i + \Omega^2\gamma_i]\sin(\psi_i) + c_{22}\dot{\phi}_X - c_{12}\dot{Y} + k_{22}\phi_X - k_{12}Y = 0. \tag{18}$$

- Sixth equation (torsional rotation ϕ_z about z-axis)

$$\ddot{\phi}_z J_p + m(l+r)\sum_{i=1}^{n}\{[\ddot{\phi}_z(l+r) + \ddot{\phi}_i l] - \ddot{X}\sin(\theta_i) + \ddot{Y}\cos(\theta_i)\} + c_t\dot{\phi}_z + k_t\phi_z = 0, \tag{19}$$

i.e.,

$$\ddot{\phi}_z J_{p_T} + ml(l+r)\sum_{i=1}^{n}\ddot{\phi}_i + c_t\dot{\phi}_z + k_t\phi_z = 0. \tag{20}$$

- Following n equations, from the seventh to the $(6+n)$th (in-plane rotations ϕ_i)

$$-\ddot{X}\sin(\theta_i) + \ddot{Y}\cos(\theta_i) + \ddot{\phi}_z(l+r) + \ddot{\phi}_i l + \left(\Omega^2 r + \frac{k_p}{ml}\right)\phi_i + \frac{l}{m}(c_p + 2c_q)\dot{\phi}_i - \frac{lc_q}{m}\dot{\phi}_{i-1} - \frac{lc_q}{m}\dot{\phi}_{i+1} = 0 \quad \text{for } i = 1, \ldots, n, \tag{21}$$

where $\dot{\phi}_{n+1} = \dot{\phi}_1$ and $\dot{\phi}_0 = \dot{\phi}_n$, i.e.,

$$[-\ddot{X}\sin(\psi_i) + \ddot{Y}\cos(\psi_i)]\cos(\Omega t) + [-\ddot{X}\cos(\psi_i) - \ddot{Y}\sin(\psi_i)]\sin(\Omega t) + \ddot{\phi}_z(l+r) + \ddot{\phi}_i l + \left(\Omega^2 r + \frac{k_p}{ml}\right)\phi_i + \frac{l}{m}(c_p + 2c_q)\dot{\phi}_i - \frac{lc_q}{m}\dot{\phi}_{i-1} - \frac{lc_q}{m}\dot{\phi}_{i+1} = 0. \tag{22}$$

- Last n equations from the $(7+n)$th to the $(6+2n)$th (out-of-plane rotations γ_i)

$$\ddot{Z} + l\ddot{\gamma} + (-\ddot{\phi}_y + 2\Omega\dot{\phi}_X)(r+l)\cos(\theta_i) + (\ddot{\phi}_X + 2\Omega\dot{\phi}_y)(r+l)\sin(\theta_i) + \gamma_i\left[\Omega^2(r+l) + \frac{k_p}{ml}\right] + \frac{l}{m}(c_p + 2c_q)\dot{\gamma}_i - \frac{lc_q}{m}\gamma_{i-1} - \frac{lc_q}{m}\dot{\gamma}_{i+1} = 0 \tag{23}$$

for $i = 1, \ldots, n$, i.e.,

$$(l+r)[-(\ddot{\phi}_y - 2\Omega\dot{\phi}_X)\cos(\psi_i) + (\ddot{\phi}_X + 2\Omega\dot{\phi}_y)\sin(\psi_i)]\cos(\Omega t) + (l+r)[(\ddot{\phi}_y - 2\Omega\dot{\phi}_X)\sin(\psi_i) + (\ddot{\phi}_X + 2\,\Omega\dot{\phi}_y)\cos(\psi_i)]\sin(\Omega t) + \ddot{Z} + l\ddot{\gamma} + \gamma_i\left[\Omega^2(l+r) + \frac{k_p}{ml}\right] + \frac{l}{m}(c_p + 2c_q)\dot{\gamma}_i - \frac{lc_q}{m}\dot{\gamma}_{i-1} - \frac{lc_q}{m}\dot{\gamma}_{i+1} = 0. \tag{24}$$

2.4. From pendulum co-ordinates to array co-ordinates

It is possible to simplify substantially the equations of motion by applying the co-ordinate transformation

$$\begin{aligned} l\phi_i &= u_0 + u_1\cos(\psi_i) + u_2\sin(\psi_i) + u_3\cos(2\psi_i) + u_4\sin(2\psi_i) + \cdots \\ l\gamma_i &= v_0 + v_1\cos(\psi_i) + v_2\sin(\psi_i) + v_3\cos(2\psi_i) + v_4\sin(2\psi_i) + \cdots . \end{aligned} \tag{25}$$

This transformation can be written in the form

$$\boldsymbol{\phi} = \begin{Bmatrix} \phi_1 \\ \phi_2 \\ \phi_3 \\ \cdots \end{Bmatrix} = \frac{1}{l}\begin{bmatrix} 1\cos(\psi_1) & \sin(\psi_1) & \cdots \\ 1\cos(\psi_2) & \sin(\psi_2) & \cdots \\ 1\cos(\psi_3) & \sin(\psi_3) & \cdots \\ \cdots & \cdots & \cdots \end{bmatrix}\begin{Bmatrix} u_0 \\ u_1 \\ u_2 \\ \cdots \end{Bmatrix} = \mathbf{Tu} \tag{26}$$

and, with obvious meaning of the notation,

$$\boldsymbol{\gamma} = \mathbf{Tv}. \tag{27}$$

The transformation matrix $\mathbf{T}$ must be square, so that the number of harmonics to be considered depends on the number of the pendulums. Consider for instance the case $n = 4$: angles ψ_i

are 0, $\pi/2$, π and $3\pi/2$ and matrix $\mathbf{T}$ is

$$\mathbf{T} = \frac{1}{l}\begin{bmatrix} 1 & 1 & 0 & 1 \\ 1 & 0 & 1 & -1 \\ 1 & -1 & 0 & 1 \\ 1 & 0 & -1 & -1 \end{bmatrix}.$$

By inverting the transformation matrix, it is possible to write

$$\begin{Bmatrix} u_0 \\ u_1 \\ u_2 \\ \dots \end{Bmatrix} = \frac{l}{n}\begin{bmatrix} 1 & 1 & 1 & \dots \\ h\cos(\psi_1) & h\cos(\psi_2) & h\cos(\psi_2) & \dots \\ h\sin(\psi_1) & h\sin(\psi_2) & h\sin(\psi_2) & \dots \\ h\cos(2\psi_1) & h\cos(2\psi_2) & h\cos(2\psi_3) & \dots \\ \dots & \dots & \dots & \dots \end{bmatrix}\begin{Bmatrix} \phi_1 \\ \phi_2 \\ \phi_3 \\ \dots \end{Bmatrix}, \tag{28}$$

where $h = 2$ everywhere, except for the last row in which $h = 2$ if n is odd and $h = 1$ if n is even. The same holds for out-of-plane rotations.

The motions described by co-ordinates u_0 and v_0 are motions with all pendulums oscillating in phase (Fig. 2a, for the case of 4 pendulums oscillating in-plane). The centre of mass of the system

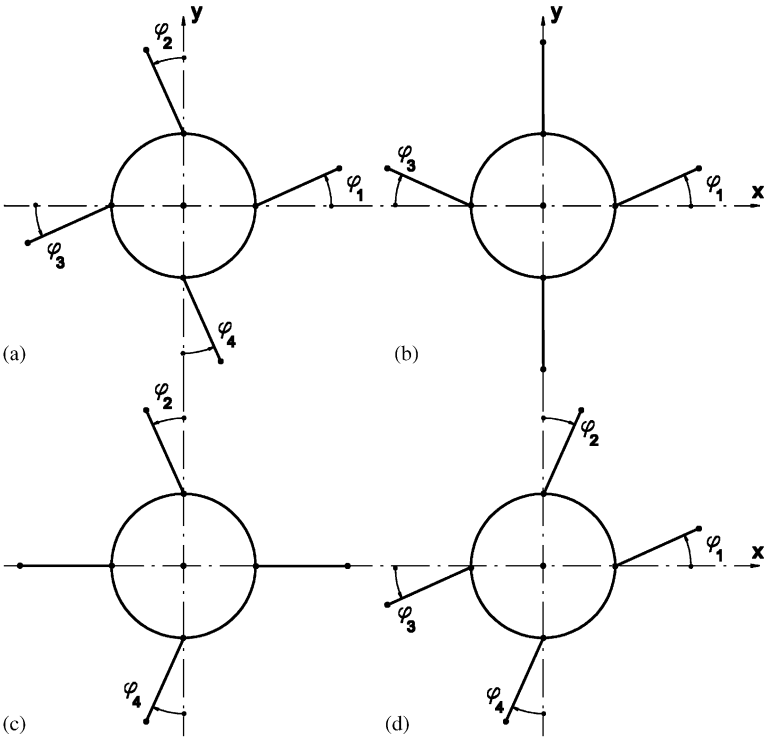

Fig. 2. Displacements of a row of four pendulums oscillating in the rotation plane of the disc corresponding to co-ordinates u_0, u_1, u_2 and u_3.

does not move and the motion is uncoupled with the lateral motions of the disc, while being coupled with its torsional (or axial, when dealing with out-of-plane oscillations) oscillations.

The second and third co-ordinates u_1 and u_2 (Figs. 2b and c) (or v_1 and v_2) undergo motions with two of the pendulums moving with 180° phasing with each other while the other two do not move. In case of in-plane oscillations these modes cause a shift of the centre of mass in Y and X directions and are coupled with displacements of the disc along Y and X axes, respectively. In the case of out-of-plane oscillations they couple with rotations of the rigid body about X and Y axes.

The fourth co-ordinate u_3 (Fig. 2d) (or v_3) regards a motion with the pendulums moving at 180° phasing with each other. No inertia reaction is exerted on the disc (if it is considered as a rigid body) and hence it is uncoupled with the dynamics of the latter. The same holds for all the other co-ordinates which would have existed if there were more than four pendulums.

- First equation (X co-ordinate)

By inspecting Eq. (28) it is clear that the sums appearing in Eq. (10) are co-ordinates u_1 and u_2 and their time derivatives. The latter reduces to

$$m_T\ddot{X} + \frac{nm}{2}(-\ddot{u}_1 + \Omega^2 u_1 + 2\Omega\dot{u}_2)\sin(\Omega t) + \frac{nm}{2}(-\ddot{u}_2 + \Omega^2 u_2 - 2\Omega\dot{u}_1)\cos(\Omega t) + c_{11}\dot{X} + c_{12}\dot{\phi}_y + k_{11}X + k_{12}\phi_y = 0. \tag{29}$$

Note that in the inertial terms of this equation only three generalized co-ordinates are present X, u_1 and u_2 while in the elastic and damping terms ϕ_y also appears. Moreover, the equation is linear but the coefficients are periodic in time through angle Ωt.

- Second equation (Y co-ordinate)

A similar consideration holds for the second equation, which also contains only four generalized co-ordinates; in this case y, u_1, u_2 and ϕ_X:

$$m_T\ddot{Y} - \frac{nm}{2}(-\ddot{u}_1 + \Omega^2 u_1 + 2\Omega\dot{u}_2)\cos(\Omega t) + \frac{nm}{2}(-\ddot{u}_2 + \Omega^2 u_2 - 2\Omega\dot{u}_1)\sin(\Omega t) + c_{11}\dot{Y} - c_{12}\dot{\phi}_X + k_{11}Y - k_{12}\phi_X = 0. \tag{30}$$

- Third equation (Z co-ordinate)

$$m_T\ddot{Z} + nm\ddot{v}_0 + c_a\dot{Z} + k_a Z = 0. \tag{31}$$

The third equation contains only the generalized co-ordinates Z and v_0; moreover it is a constant coefficients linear equation.

- Fourth equation (ϕ_y co-ordinate)

$$\ddot{\phi}_y J_{t_T} - \Omega\dot{\phi}_X J_{p_T} - \frac{mn}{2}(1+\delta)(\ddot{v}_1 + \Omega^2 v_1)\cos(\Omega t) + \frac{mn}{2}(1+\delta)(\ddot{v}_2 + \Omega^2 v_2)\sin(\Omega t) + c_{11}\dot{\phi}_y + c_{12}\dot{X} + k_{11}\phi_y + k_{12}X = 0, \tag{32}$$

where

$$\delta = \frac{r}{l} \quad (0 < \delta < \infty). \tag{33}$$

- Fifth equation (ϕ_X co-ordinate)

$$\ddot{\phi}_X J_{t_T} + \Omega \dot{\phi}_y J_{p_T} + \frac{mn}{2}(1+\delta)(\ddot{v}_1 + \Omega^2 v_1)\sin(\Omega t) + \frac{mn}{2}(1+\delta)(\ddot{v}_2 + \Omega^2 v_2)\cos(\Omega t) + c_{22}\dot{\phi}_X - c_{12}\dot{Y} + k_{22}\phi_X - k_{12}Y = 0. \tag{34}$$

- Sixth equation (ϕ_z co-ordinate)

$$\ddot{\phi}_z J_{p_T} + nml(1+\delta)\ddot{u}_0 + c_t\dot{\phi}_z + k_t\phi_z = 0. \tag{35}$$

- Equations from the seventh to the $(6+n)$th (co-ordinates u_i).

The other n equations (22) can be substituted by their linear combinations

$$\mathbf{T}^{-1}\mathbf{p} = 0, \tag{36}$$

where $\mathbf{T}$ is the co-ordinate transformation matrix defined in Eq. (26) and p_i is the right-hand side of the generic ith equation of this group.

The first transformed equation (seventh equation) reduces to

$$l\ddot{\phi}_z(1+\delta) + \ddot{u}_0 + \frac{c_p}{m}\dot{u}_0 + \left(\Omega^2\delta + \frac{k_p}{ml^2}\right)u_0 = 0 \tag{37}$$

and couples only to the sixth equation; moreover it does not contain any term in c_q. This was expected, since it represents a motion in which all pendulums oscillate together, with the same amplitude and phase, and hence the dampers located between the pendulums do not affect this mode. This motion couples only with the torsional vibration of the rigid body due to the compliance of the drive system.

The following two equations (Eqs. (8) and (9)) yield

$$\begin{aligned} &-\ddot{X}\sin(\Omega t) + \ddot{Y}\cos(\Omega t) + \ddot{u}_1 + \frac{1}{m}(c_p + 2c_i)\dot{u}_1 + \left(\Omega^2\delta + \frac{k_p}{ml^2}\right)u_1 \\ &\quad - \frac{c_q l}{nm}\sum_{i=1}^{n}\dot{\phi}_i[\cos(\psi_{i+1}) + \cos(\psi_{i-1})] = 0, \\ &-\ddot{X}\cos(\Omega t) - \ddot{Y}\sin(\Omega t) + \ddot{u}_2 + \frac{1}{m}(c_p + 2c_i)\dot{u}_2 + \left(\Omega^2\delta + \frac{k_p}{ml^2}\right)u_2 \\ &\quad - \frac{c_q l}{nm}\sum_{i=1}^{n}\dot{\phi}_i[\sin(\psi_{i+1}) + \sin(\psi_{i-1})] = 0. \end{aligned} \tag{38}$$

By remembering that $\psi_{i+1} = \psi_i + \Delta\psi$ and $\psi_{i-1} = \psi_i - \Delta\psi$ (angle $\Delta\psi = 2\pi/n$ is the angle between two subsequent pendulums), they reduce to

$$
\begin{aligned}
&-\ddot{X}\sin(\Omega t) + \ddot{Y}\cos(\Omega t) + \ddot{u}_1 + \frac{1}{m}c\dot{u}_1 + \left(\Omega^2\delta + \frac{k_p}{ml^2}\right)u_1 = 0,\\
&-\ddot{X}\cos(\Omega t) - \ddot{Y}\sin(\Omega t) + \ddot{u}_2 + \frac{1}{m}c\dot{u}_2 + \left(\Omega^2\delta + \frac{k_p}{ml^2}\right)u_2 = 0,
\end{aligned}
\tag{39}
$$

where

$$
c = c_p + 2c_q[1 - \cos(\Delta\psi)] = c_p + 4c_i \sin^2\left(\frac{\Delta\psi}{2}\right). \tag{40}
$$

They are inertially coupled with the first two equations, showing that the motion with all pendulums following a pattern of the type shown in Figs. 2b and c is coupled with the motion of the disc.

The remaining equations, from the fourth one to the nth of this group (equation from the tenth to $(6+n)$th) are of the type

$$
\begin{aligned}
&\ddot{u}_3 + \frac{1}{m}[c_p + 4c_q \sin^2(\Delta\psi)]\dot{u}_3 + \left(\Omega^2\delta + \frac{k_p}{ml^2}\right)u_3 = 0,\\
&\ddot{u}_4 + \frac{1}{m}[c_p + 4c_q \sin^2(\Delta\psi)]\dot{u}_4 + \left(\Omega^2\delta + \frac{k_p}{ml^2}\right)u_4 = 0,\\
&\ddot{u}_5 + \frac{1}{m}\left[c_p + 4c_q \sin^2\left(\frac{3}{2}\Delta\psi\right)\right]\dot{u}_5 + \left(\Omega^2\delta + \frac{k_p}{ml^2}\right)u_5 = 0.
\end{aligned}
\tag{41}
$$

These equations are uncoupled with each other and with all other ones and describe the motions of the pendulums with different phasing. These equations are all equal, except for the role played by damping c_q: which increases with increasing order of the equations. If the pendulums are many, the damping coefficient appearing in the last equation, that dealing with the variable u_{n-1}, is $c_p + 4c_q$.

They show that all motions following a pattern of the type shown in Fig. 2d, i.e. with the centre of mass of the system of the pendulums stationary in the centre of the disc, are uncoupled with the motion of the latter.

- Last n equations from the $(7+n)$th to the $(6+2n)$th (co-ordinates v_i).

These n equations can be combined linearly as seen for the case of the equations of the former group (36).

The first of the combined equations (Eq. $(7+n)$) describes the motion with all pendulums oscillating in phase

$$
\ddot{Z} + \ddot{v}_0 + \frac{c_p}{m}\dot{v}_0 + \left[\Omega^2(1+\delta) + \frac{k_p}{ml^2}\right]v_0 = 0. \tag{42}
$$

It couples only with the third equation and describes the axial dynamics of the system.

The following two equations (Eqs. $(8+n)$ and $(9+n)$) are inertially coupled with the first, fourth and fifth equations (those dealing with the conical motion of the rigid rotor). Operating in

the same way as before, and introducing the damping coefficient c expressed by Eq. (40), it follows

$$\begin{aligned}
&(\delta+1)[-(\ddot{\phi}_y - 2\Omega\dot{\phi}_X)]\cos(\Omega t) + (\delta+1)[(\ddot{\phi}_X + 2\Omega\dot{\phi}_y)]\sin(\Omega t)\\
&\quad + \frac{1}{l}\ddot{v}_1 + \frac{c}{ml}\dot{v}_1 + \frac{1}{l}\left[\Omega^2(\delta+1) + \frac{k_p}{ml^2}\right]v_1 = 0,\\
&(\delta+1)[(\ddot{\phi}_X + 2\Omega\dot{\phi}_y)]\cos(\Omega t) + (\delta+1)[(\ddot{\phi}_y - 2\Omega\dot{\phi}_X)]\sin(\Omega t)\\
&\quad + \frac{1}{l}\ddot{v}_2 + \frac{c}{ml}\dot{v}_2 + \frac{1}{l}[\Omega^2(\delta+1) + \frac{k_p}{ml^2}]v_2 = 0.
\end{aligned} \tag{43}$$

All the following equations (Eqs. $(10+n)$ to $(6+2n)$) do not contain either ϕ_X or ϕ_y. They are all of the type

$$\ddot{v}_i + \frac{c^*}{m}\dot{v}_i + \left[\Omega^2(\delta+1) + \frac{k_p}{ml^2}\right]v_i = 0 \quad \text{for } i = 3, \ldots, n-1, \tag{44}$$

where c^* is a damping coefficient of the type appearing in Eq. (41), showing that the damping located between the pendulums is more important in the equations with a high value of i. Since they are uncoupled with the other ones, these equations will not be dealt with any further.

The disc–pendulums interaction can thus be studied using a set of 12 linear equations (with periodic coefficients) in the six generalized co-ordinates of the rigid rotor, plus u_0, u_1, u_2, v_0, v_1 and v_2.

2.5. Axial dynamics

The axial dynamics of the system can be studied by resorting to the third and $(7+n)$th equations (31) and (42)

$$\begin{aligned}
&\begin{bmatrix} m_T & nm \\ nm & nm \end{bmatrix}\begin{Bmatrix} \ddot{Z} \\ \ddot{v}_0 \end{Bmatrix} + \begin{bmatrix} c_a & 0 \\ 0 & nc_p \end{bmatrix}\begin{Bmatrix} \dot{Z} \\ \dot{v}_0 \end{Bmatrix}\\
&\quad + \begin{bmatrix} k_a & 0 \\ 0 & nm[\Omega^2(1+\delta) + \frac{k_p}{ml^2}] \end{bmatrix}\begin{Bmatrix} Z \\ v_0 \end{Bmatrix} = \mathbf{0}.
\end{aligned} \tag{45}$$

By introducing the non-dimensional parameters

$$\alpha_1 = \frac{nm}{m_T} \quad (0<\alpha<1) \quad \text{and} \quad \Omega^* = \frac{\Omega}{\omega_{ax}}, \tag{46}$$

where ω_{ax} is the axial natural frequency of the system with the pendulums locked expressed by Eq. (4), the equation of motion of the undamped system with no restoring spring can be written in the form

$$\begin{bmatrix} 1 & \alpha_1 \\ \alpha_1 & \alpha_1 \end{bmatrix}\begin{Bmatrix} \ddot{Z} \\ \ddot{v}_0 \end{Bmatrix} + \omega_{ax}^2\begin{bmatrix} 1 & 0 \\ 0 & \alpha_1\Omega^{*^2}(1+\delta) \end{bmatrix}\begin{Bmatrix} Z \\ v_0 \end{Bmatrix} = \mathbf{0}. \tag{47}$$

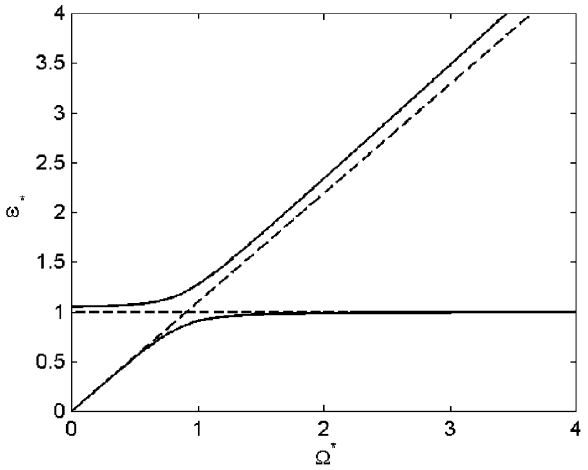

Fig. 3. Non-dimensional axial Campbell diagram for the case of pendulums with $\alpha = 0.1$ and $\delta = 0.2$ ($\omega^* = \omega/\omega_{ax}$). Dashed lines: uncoupled solution; full lines: coupled solution. Note the conservative coupling.

The natural frequencies of the undamped system are readily computed

$$\frac{\omega}{\omega_{ax}} = \sqrt{\frac{1 + \Omega^{*^2}(1+\delta) \pm \sqrt{[1 + \Omega^{*^2}(1+\delta)]^2 - 4\Omega^{*^2}(1+\delta)(1-\alpha_1)}}{2(1-\alpha_1)}}. \tag{48}$$

A non-dimensional Campbell diagram, plotted for $\alpha_1 = 0.1$ and $\delta = 0.2$ is shown in Fig. 3. A value $\alpha_1 = 0.1$ corresponds to quite light pendulums, having a total mass nm equal to one-ninth of the mass of the disc ($nm = m_d/9$), while $\delta = 0.2$ corresponds to fairly long pendulums. The coupled dynamics (full lines) is compared with the uncoupled dynamics (dashed lines). From the figure it is clear that the coupling is *repulsive* (or conservative) [7] and that there is no field of instability. By looking at the structure of the complete equation, it is clear that damping has the usual role seen in structural dynamics, and that there is no danger of instability. Axial dynamics will not be dealt with any further.

2.6. Torsional dynamics

The torsional dynamics of the system can be studied by resorting to the sixth and seventh equations (35) and (37)

$$\begin{bmatrix} J_{p_T} & nml(1+\delta) \\ mnl(1+\delta) & nm \end{bmatrix} \begin{Bmatrix} \ddot{\phi}_z \\ \ddot{u}_0 \end{Bmatrix} + \begin{bmatrix} c_t & 0 \\ 0 & nc_p \end{bmatrix} \begin{Bmatrix} \dot{\phi}_z \\ \dot{u}_0 \end{Bmatrix} + \begin{bmatrix} k_t & 0 \\ 0 & n(m\Omega^2 + \frac{k_p}{l^2}) \end{bmatrix} \begin{Bmatrix} \phi_z \\ u_0 \end{Bmatrix} = \mathbf{0}. \tag{49}$$

The equation has a structure which is very similar to that seen for axial dynamics, and the same conclusions also hold for this case. Note that there is no difference whether the damping of the torsional vibration of the rigid rotor (damping coefficient c_t) acts on the rotor or on the stator of the machine. This is a known result. Also torsional dynamics will not be dealt with any further.

2.7. Lateral dynamics

The study of the lateral dynamics of the system can be performed by using eight equations: (1), (2), (4), (5), (8), (9), $(n+8)$ and $(n+9)$. They are all equations with periodic coefficients.

The physical meaning of u_1 and u_2 is straightforward. Each of the terms which are added to yield u_1 and u_2 in Eq. (28) are the projections of the displacements in the direction of the rotating axes ξ and η of point P_i, divided by 2, when the centre of the support is locked in its rest position. After adding all the terms, what is obtained is the displacement (divided by $n/2$) of the centre of mass of the pendulums when they move following the pattern of Fig. 2b and c.

This set of eight equations can be transformed into a set of constant coefficients equations by resorting to a further change of co-ordinates:

$$\begin{aligned} X_1 &= -u_2\cos(\Omega t) - u_1\sin(\Omega t),\\ Y_1 &= u_1\cos(\Omega t) - u_2\sin(\Omega t) \end{aligned} \tag{50}$$

which amounts to writing the displacement of the centre of mass of the pendulums in an inertial frame instead of writing it with reference to the rotor fixed frame, and

$$\begin{aligned} \phi_{y1} &= \frac{1}{l}[-v_1\cos(\Omega t) + v_2\sin(\Omega t)],\\ \phi_{X1} &= \frac{1}{l}[v_1\sin(\Omega t) + v_2\cos(\Omega t)]. \end{aligned} \tag{51}$$

By performing the relevant computations and reordering the equations, they transform into

$$\begin{aligned}
&m_T\ddot{X} + \frac{nm}{2}\ddot{X}_1 + c_{11}\dot{X} + c_{12}\dot{\phi}_y + k_{11}X + k_{12}\phi_y = 0,\\
&m_T\ddot{Y} + \frac{nm}{2}\ddot{Y}_1 + c_{11}\dot{Y} - c_{12}\dot{\phi}_X + k_{11}Y - k_{12}\phi_X = 0,\\
&\ddot{X} + \ddot{X}_1 + 2\Omega\dot{Y}_1 + \frac{c}{m}\dot{X}_1 + \left[\Omega^2(\delta-1) + \frac{k_p}{ml^2}\right]X_1 + \Omega\frac{c}{m}Y_1 = 0,\\
&\ddot{Y} + \ddot{Y}_1 - 2\Omega\dot{X}_1 + \frac{c}{m}\dot{Y}_1 + \left[\Omega^2(\delta-1) + \frac{k_p}{ml^2}\right]Y_1 - \Omega\frac{c}{m}X_1 = 0,\\
&\ddot{\phi}_y J_{t_T} - \Omega\dot{\phi}_X J_{p_T} + \ddot{\phi}_{y1}J_m - 2\Omega\dot{\phi}_{X1}J_m + c_{11}\dot{\phi}_y + c_{12}\dot{X} + k_{11}\phi_y + k_{12}X = 0,\\
&\ddot{\phi}_X J_{t_T} + \Omega\dot{\phi}_y J_{p_T} + \ddot{\phi}_{X1}J_m + 2\Omega\dot{\phi}_{y1}J_m + c_{22}\dot{\phi}_X - c_{12}\dot{Y} + k_{22}\phi_X - k_{12}Y = 0,\\
&(\delta+1)(\ddot{\phi}_y - 2\Omega\dot{\phi}_X) + \ddot{\phi}_{y1} - 2\Omega\dot{\phi}_{X1} + \frac{c}{m}(\dot{\phi}_{y1} - \Omega\phi_{X1})\\
&\quad + \left[\Omega^2\delta + \frac{k_p}{ml^2}\right]\phi_{y1} = 0,
\end{aligned}$$

$$(\delta+1)(\ddot{\phi}_X+2\Omega\dot{\phi}_y)+\ddot{\phi}_{X1}+2\Omega\dot{\phi}_{y1}+\frac{c}{m}(\dot{\phi}_{X1}+\Omega\phi_{y1})+\left[\Omega^2\delta+\frac{k_p}{ml^2}\right]\phi_{X1}=0, \tag{52}$$

where

$$J_m=\frac{nml^2}{2}(1+\delta).$$

This set of equations can be further simplified by resorting to complex co-ordinates

$$r_d=X+\mathrm{j}Y,\quad \phi_d=\phi_y-\mathrm{j}\phi_X,$$
$$r_p=X_1+\mathrm{j}Y_1,\quad \phi_p=\phi_{y1}-\mathrm{j}\phi_{X1}, \tag{53}$$

where $\mathrm{j}=\sqrt{-1}$ is the imaginary unit.

By adding the first equation to the second multiplied by j and the third one to the fourth multiplied by j, it follows

$$m_T\ddot{r}_d+\frac{nm}{2}\ddot{r}_p+c_{11}\dot{r}_d+c_{12}\dot{\phi}_d+k_{11}r_d+k_{12}\phi_d=0,$$
$$\ddot{r}_d+\ddot{r}_p+\left(\frac{c}{m}-2\mathrm{j}\Omega\right)\dot{r}_p+\left[\Omega^2(\delta-1)+\frac{k_p}{ml^2}-\mathrm{j}\Omega\frac{c}{m}\right]r_p=0. \tag{54}$$

Finally, by adding the fifth equation to the sixth multiplied by $-\mathrm{j}$ and the seventh one to the eighth multiplied by $-\mathrm{j}$, it follows

$$\ddot{\phi}_d J_{t_T}-\mathrm{j}\Omega\dot{\phi}_d J_{p_T}+\ddot{\phi}_p J_m-2\mathrm{j}\Omega\dot{\phi}_p J_m+c_{12}\dot{r}_d+c_{22}\dot{\phi}_d+k_{12}r_d+k_{22}\phi_d=0,$$
$$(\delta+1)(\ddot{\phi}_d-2\mathrm{j}\Omega\dot{\phi}_d)+\ddot{\phi}_p+\left(\frac{c}{m}-2\mathrm{j}\Omega\right)\dot{\phi}_p+\left[\Omega^2\delta+\frac{k_p}{ml^2}-\mathrm{j}\Omega\frac{c}{m}\right]\phi_p=0. \tag{55}$$

The set of two equations (54) deals with the in-plane behaviour of the system, while set (55) deals with the out-of-plane behaviour. They are coupled by the damping terms in c_{12} and by the elastic terms in k_{12}.

Assuming that these terms are vanishingly small, the in-plane and the out-of-plane behaviour decouple.

Note that the damping of the pendulums c plays in these equations the classical role of rotating damping: it appears in the terms in the generalized velocities (i.e., in the damping matrix of the system), but also in the terms in the generalized displacements (i.e., in the circulatory matrix of the system). Note also that a gyroscopic term is present in all equations except the first one.

2.7.1. In-plane dynamics

Consider the in-plane dynamics of the system. To assess the inertial coupling effects, firstly the undamped system with no restoring spring at the pendulums will be studied. By stating $k_{11}=0$ and $c_{11}=c=0$ and by introducing the non-dimensional parameter

$$\alpha_2=\frac{nm}{2m_T}\quad\left(0<\alpha_2<\frac{1}{2}\right) \tag{56}$$

the equation of motion can be written in the form

$$\begin{bmatrix} 1 & \alpha_2 \\ \alpha_2 & \alpha_2 \end{bmatrix} \begin{Bmatrix} \ddot{r}_d \\ \ddot{r}_p \end{Bmatrix} - 2\mathrm{j}\Omega\alpha_2 \begin{bmatrix} 0 & 0 \\ 0 & 1 \end{bmatrix} \begin{Bmatrix} \dot{r}_d \\ \dot{r}_p \end{Bmatrix} + \begin{bmatrix} \omega_1 & 0 \\ 0 & \Omega^2\alpha_2(\delta-1) \end{bmatrix} \begin{Bmatrix} r_d \\ r_p \end{Bmatrix} = \mathbf{0}, \tag{57}$$

where $\omega_1 = \sqrt{k_{11}/m_T}$ is the natural frequency of mass m_T on a spring with stiffness k_{11}.

By introducing the non-dimensional speed and Laplace variable

$$\Omega^* = \frac{\Omega}{\omega_1}, \quad s^* = \frac{s}{\omega_1} \tag{58}$$

a non-dimensional response depending only on α_2 and δ can be obtained from the characteristic equation

$$\det \begin{bmatrix} s^{*2}+1 & s^{*2}\alpha_2 \\ s^{*2}\alpha_2 & \alpha_2[s^{*2} - 2\mathrm{j}\Omega^* s^* + \Omega^{*2}(\delta-1)] \end{bmatrix} = 0. \tag{59}$$

By inspecting the stiffness matrix of the system it is clear that the condition $\delta = 1$, i.e., $r = l$, is peculiar, since it corresponds to a singular stiffness matrix. Two cases can be defined:

- short pendulums, $l < r$ (i.e., $\delta > 1$), where the stiffness matrix is positive defined, and
- long pendulums, $l > r$ (i.e., $\delta < 1$), where the stiffness matrix is negative defined.

Before attempting to solve Eq. (59), an approximate solution can be obtained by neglecting the terms outside the main diagonal. The uncoupled dynamics of the system can thus be studied. The first equation is

$$s^{*2} + 1 = 0. \tag{60}$$

Its solutions are

$$s^* = \pm\mathrm{j} \tag{61}$$

and correspond to the natural frequencies of the system oscillating on its supports with the pendulums locked.

The second equation

$$s^{*2} - 2\mathrm{j}\Omega^* s^* + \Omega^{*2}(\delta-1) = 0 \tag{62}$$

yields the solutions

$$s^* = \mathrm{j}\Omega^*(1 \pm \sqrt{\delta}) \tag{63}$$

and corresponds to the natural frequencies of the pendulums oscillating on the locked support. This is fully consistent with the well-known result (Eq. (1)) for the in-plane natural frequency ω_{ip} of rotating pendulums, provided that it is accounted for that Eq. (1) is written with reference to the rotating (rotor-fixed) frame, while Eq. (63) refers to the fixed (stator-fixed) frame.

In the rotating frame the global motion of the pendulum array can be seen as a forward moving wave, propagating at an angular velocity ω_{ip} plus a backward moving wave, propagating at an angular velocity $-\omega_{ip}$. The forward moving wave is seen in the fixed frame as a wave propagating

in a forward direction with a speed $\Omega + \omega_{ip} = \Omega(1 + \sqrt{\delta})$, which coincides with the solution with (+) in Eq. (63).

The backward wave is seen as in the fixed frame as a wave propagating with a speed $\Omega - \omega_{ip} = \Omega(1 - \sqrt{\delta})$, coinciding with the solution with (−) in Eq. (63). This wave propagates in a forward direction if $\delta < 1$, i.e., in the case of long pendulums, and in a backward direction if $\delta > 1$, i.e., in the case of short pendulums.

The non-dimensional Campbell diagram and the decay rate plot for the case of a long pendulum with $\alpha = 0.1$ and $\delta = 0.2$ are shown in Fig. 4a and b. A value $\alpha = 0.1$ corresponds to pendulums having a total mass nm equal to one quarter of the mass of the disc ($nm = 0.25m_d$). A field of instability, with a threshold at $\Omega^* = 1.24$ is present. Note that, as expected, the threshold of instability is located in the supercritical field.

A similar non-dimensional Campbell diagram, but for the case of a short pendulum with $\alpha = 0.1$ and $\delta = 2$ is reported in Fig. 4c. Here no instability range is present.

Numerical experimentation has shown that the field of instability is present wherever the travelling wave which moves backwards in the rotating frame, moves forward in the fixed frame, i.e., in the case of long pendulums ($\delta < 1$). The value of α affects the width of the instability range, but not its presence. No instability was found for the case of the short pendulum ($\delta > 1$).

This field of instability has nothing to do with rotating damping or with the circulatory matrix, which has not been accounted for in the undamped model, but is due to the stiffness matrix, which may not be positive definite.

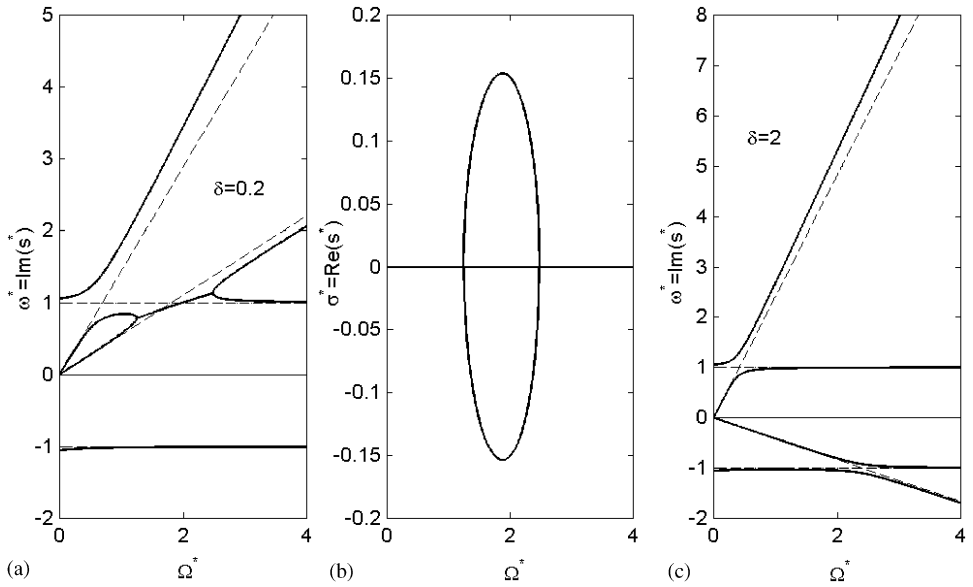

Fig. 4. (a) and (b) Campbell diagram and decay rate plot for the case of long undamped pendulums without restoring springs, with $\alpha = 0.1$ and $\delta = 0.2$. Note the field of instability. (c) Campbell diagram and decay rate plot for the case of short pendulums with $\alpha = 0.1$ and $\delta = 2$. In this case no field of instability exists. Dashed lines: uncoupled solution; full lines: coupled solution. Note the non-conservative coupling in (a).

The presence of the spring introduces a further parameter, for example

$$\omega_p^* = \frac{\omega_p}{\omega_1}, \tag{64}$$

where $\omega_p = \sqrt{k_p/ml^2}$ is the natural frequence of the pendulums at standstill (neglecting the gravitational acceleration as consistent with the whole study), but does not change the overall picture.

When damping is considered, two further parameters

$$\zeta_d = \frac{c_{11}}{2\sqrt{k_{11}m_T}} \quad \text{and} \quad \zeta_p = \frac{m_T}{m}\frac{c_p + 4c_q \sin^2(\Delta\psi/2)}{2\sqrt{km_T}} \tag{65}$$

must be introduced.

The characteristic equation yielding the non-dimensional natural frequencies then becomes

$$\det\begin{bmatrix} s^{*2} + 2s^*\zeta_d + 1 & s^{*2}\alpha \\ s^{*2}\alpha & \alpha[s^{*2} + 2s^*\zeta_p + \Omega^{*2}(\delta - 1) + \omega_p^{*2} - 2\mathrm{j}\Omega^*(s^* + \zeta_p)] \end{bmatrix} = 0. \tag{66}$$

The uncoupled dynamics is easily studied. The motion of the system with the pendulums locked is equivalent to that of a Jeffcott rotor with no rotating damping, and, assuming that the system is underdamped ($\zeta_d < 1$), the solutions for s^* are

$$s^* = -\zeta_d \pm \mathrm{j}\sqrt{1 - \zeta_d^2}. \tag{67}$$

The real part of s^* is always negative, and the system is stable.

The motion of the pendulums on the locked support is governed by equation

$$s^{*2} + 2(\zeta_p - \mathrm{j}\Omega^*)s^* + \Omega^{*2}(\delta - 1) + \omega_p^{*2} - 2\mathrm{j}\Omega^*\zeta_p = 0 \tag{68}$$

yielding

$$s^* = -\zeta_p + \mathrm{j}\Omega^* \pm \sqrt{\zeta_p^2 - \delta\Omega^{*2} - \omega_p^{*2}}. \tag{69}$$

Here there are two cases: if the damping is low, i.e., if $\zeta_p^2 < \delta\Omega^{*2} - \omega_p^{*2}$, the solutions for s are

$$s^* = -\zeta_p + \mathrm{j}(\Omega^* \pm \sqrt{\delta\Omega^{*2} + \omega_p^{*2} - \zeta_p^2}). \tag{70}$$

On the contrary, if the damping is high, i.e., if $\zeta_p^2 > \delta\Omega^{*2} - \omega_p^{*2}$, the solutions for s are

$$s^* = -\zeta_p \pm \sqrt{\zeta_p^2 - \delta\Omega^{*2} - \omega_p^{*2}} + \mathrm{j}\Omega^*. \tag{71}$$

In all cases, the real part of s^* is always negative, and the system is stable.

This is a remarkable result, since one would expect that the damping applied to the pendulums, and above all that located between them, would have an unstabilizing effect, being rotating

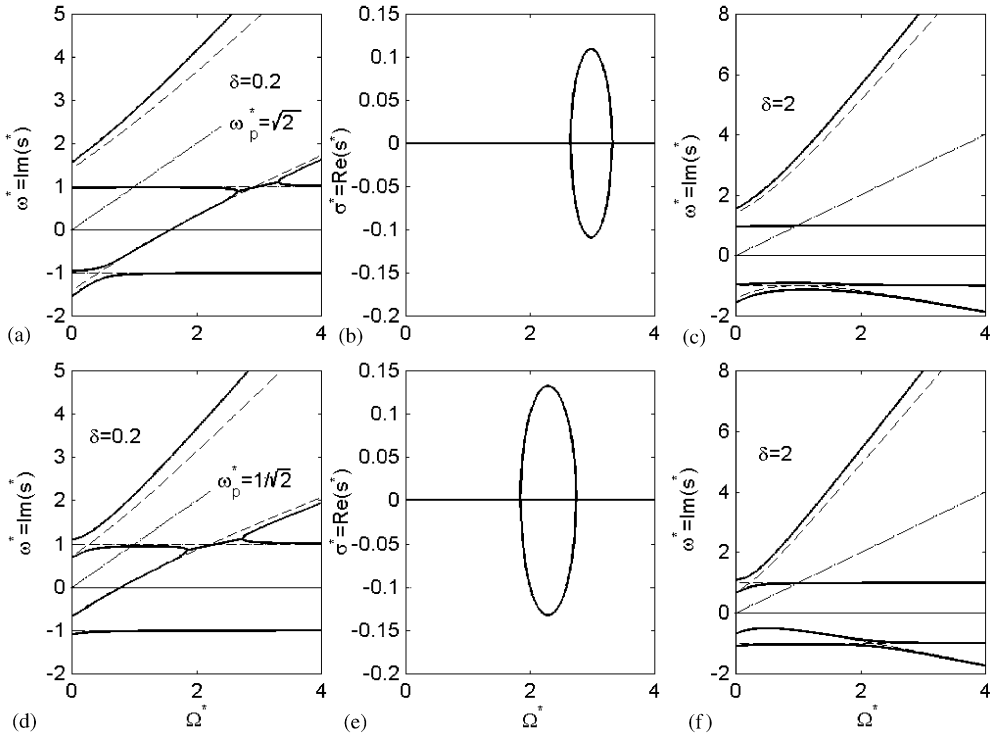

Fig. 5. Same as Fig. 4, but for pendulums with restoring springs.

damping. However, it must be remembered that this applies to the uncoupled system, and that the instability due to the coupling of the disc and pendulums dynamics is not included in it.

To study the interaction, the coupled system must be studied. Some numerical results for undamped systems are shown in Fig. 5: the non-dimensional Campbell diagram and the decay rate plot reported deal with the case of long pendulums with $\alpha = 0.1$, $\delta = 0.2$ and $\omega_p^* = \sqrt{2}$ (a and b) and $\omega_p^* = 1/\sqrt{2}$ (d and e). The system is the same as that studied in Fig. 4a and b, but with a restoring spring added. The instability ranges are clearly visible.

The same restoring springs are applied to the short pendulum of Fig. 4c. The results are reported in Fig. 5c and f and show that no instability range is present.

Cases with different combinations of non-rotating ζ_d and rotating ζ_p damping are shown in Fig. 6. The system is the long pendulums one of Fig. 4a and b. The effect of damping on the Campbell diagram is not large, since all the values of ζ used are much smaller than unity, while is important on the decay rate plot.

From the figure it is clear that with a low value of both non-rotating (disc) and rotating (pendulums) damping the field of instability, although reduced in comparison with the undamped case, is still present. An increase of any form of damping is effective in stabilizing the system, although quite a large damping is needed to cancel completely the instability range. The feature that the damping of the pendulums does not contribute to instability is thus also confirmed for the coupled system.

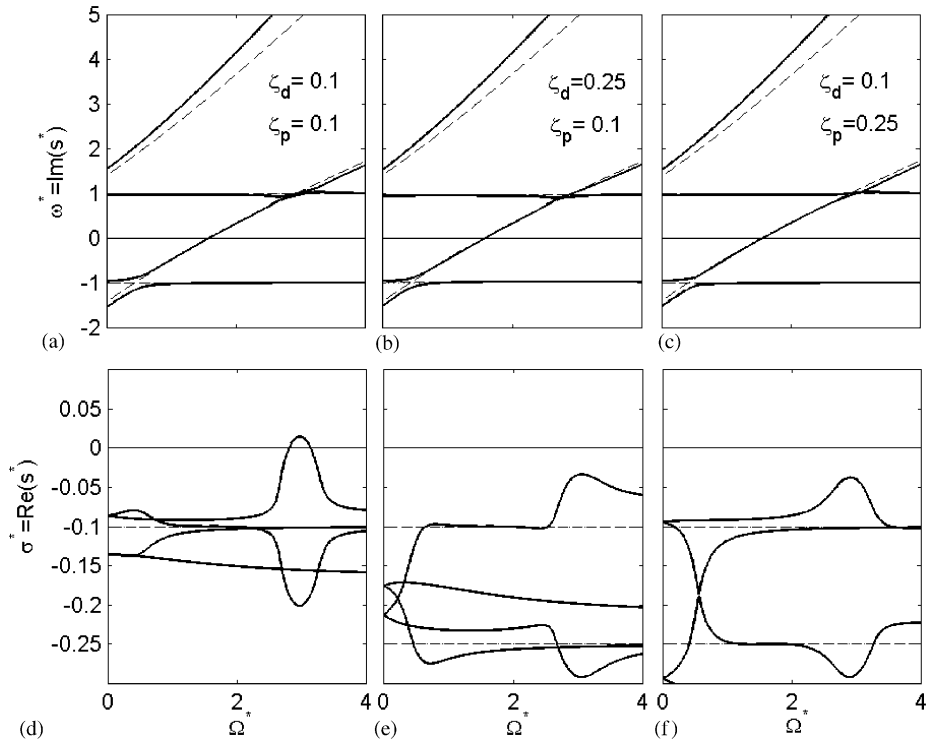

Fig. 6. Campbell diagram (a, b, c) and decay rate plot (d, e, f) for damped long pendulums with $\alpha = 0.1$, $\delta = 0.2$. and $\omega_p^* = \sqrt{2}$. Different combinations of non-rotating ζ_d and rotating ζ_p damping. Dashed lines: uncoupled solution; full lines: coupled solution.

2.7.2. *Out-of-plane dynamics*

By introducing, together with the already mentioned parameter δ, the non-dimensional parameters

$$\alpha_3 = \frac{J_m}{J_{t_T}} = \frac{nml(r+l)}{2J_t + nm(r+l)^2}, \quad \beta = \frac{J_{p_T}}{J_{t_T}},$$
$$\zeta_d = \frac{c_d}{2\sqrt{k_{22}J_{t_T}}}, \quad \zeta_p = \frac{c\sqrt{J_{t_T}}}{2m\sqrt{k_{22}}} \tag{72}$$

and the natural frequencies $\omega_1 = \sqrt{k_{22}/J_{t_T}}$ and $\omega_p = \sqrt{k_p/ml^2}$, the equation of motion can be written in the form

$$\begin{bmatrix} 1 & \alpha_3 \\ \alpha_3 & \frac{\alpha_3}{1+\delta} \end{bmatrix} \begin{Bmatrix} \ddot{\phi}_d \\ \ddot{\phi}_p \end{Bmatrix} + \left(2\omega_1 \begin{bmatrix} \zeta_d & 0 \\ 0 & \frac{\alpha_3}{(1+\delta)}\zeta_p \end{bmatrix} - \mathrm{j}\Omega \begin{bmatrix} \beta & 2\alpha_3 \\ 2\alpha_3 & \frac{2\alpha_3}{1+\delta} \end{bmatrix} \right) \begin{Bmatrix} \dot{\phi}_p \\ \dot{\phi}_d \end{Bmatrix}$$
$$+ \left(\omega_1^2 \begin{bmatrix} 1 & 0 \\ 0 & \frac{\alpha_3}{\omega_1^2(1+\delta)}(\delta\Omega^2 + \omega_p^2) \end{bmatrix} - \mathrm{j}\Omega\omega_1 \begin{bmatrix} 0 & 0 \\ 0 & \frac{2\alpha_3}{1+\delta}\zeta_p \end{bmatrix} \right) \begin{Bmatrix} \phi_d \\ \phi_p \end{Bmatrix} = \mathbf{0}. \tag{73}$$

By introducing the non-dimensional speed, Laplace variable and frequency

$$\Omega^* = \frac{\Omega}{\omega_1}, \quad s^* = \frac{s}{\omega_1}, \quad \omega_p^* = \frac{\omega_p}{\omega_1} \tag{74}$$

a non-dimensional response can be obtained from the characteristic equation

$$\det \begin{bmatrix} s^{*2} + s^*(2\zeta_d - \mathrm{j}\Omega^*\beta) + 1 & s^{*2}\alpha_3 - 2\mathrm{j}\Omega^* s^* \alpha_3 \\ s^{*2}\alpha_3 - 2\mathrm{j}\Omega^* s^* \alpha_3 & \frac{\alpha_3}{(1+\delta)}[s^{*2} + 2s^*(\zeta_p - \mathrm{j}\Omega^*) + \Omega^{*2}\delta + \omega_p^{*2} - 2\mathrm{j}\Omega^*\zeta_p] \end{bmatrix} = 0. \tag{75}$$

In this case there is no value of δ causing the stiffness matrix to be singular. In this condition there is no need to distinguish the cases of short and long pendulums.

As usual, the uncoupled problem can be solved before attempting to solve Eq. (75). The first equation is

$$s^{*2} + s^*(2\zeta_d - \mathrm{j}\Omega^*\beta) + 1 = 0. \tag{76}$$

It coincides with the equation of motion of an uncoupled system with four-degrees-of-freedom in which only non-rotating damping is present. Its solutions are

$$s^* = -\zeta_d + \mathrm{j}\Omega^* \frac{\beta}{2} \pm \sqrt{\left(\zeta_d - \mathrm{j}\Omega^* \frac{\beta}{2}\right)^2 - 1} \tag{77}$$

and no instability is obtained.

The second equation

$$s^{*2} + 2s^*(\zeta_p - \mathrm{j}\Omega^*) + \Omega^{*2}\delta + \omega_p^{*2} - 2\mathrm{j}\Omega^*\zeta_p = 0 \tag{78}$$

yields the solutions

$$s^* = -\zeta_p + \mathrm{j}\Omega^* \pm \sqrt{\zeta_p^2 - \Omega^{*2}(1+\delta) - \omega_p^{*2}}. \tag{79}$$

If damping and pendulum restoring force (stiffness k_p) are neglected, Eq. (79) reduces to

$$s^* = \mathrm{j}\Omega^*\left(1 \pm \sqrt{1+\delta}\right) \tag{80}$$

which is consistent with what has been obtained earlier on rotating pendulums: the natural frequency for out-of-plane motion, referred to the rotating frame, of a single rotating pendulum is ω_{op} defined by Eq. (2).

As in the previous case, the global motion of the pendulum array can be seen in the rotating frame as a wave, propagating in a forward direction at an angular velocity ω_{op} plus a backward wave, propagating at an angular velocity $-\omega_{op}$. The forward wave is seen in the fixed frame as a wave propagating in a forward direction with a speed $\Omega + \omega_{op} = \Omega(1 + \sqrt{\delta})$, which coincides with the solution with (+) in Eq. (80). What is different from the in-plane oscillations of the pendulums is that in the present case the backward wave is always seen in the fixed frame as a wave propagating in a backward direction. Its speed is $\Omega - \omega_{op} = \Omega(1 - \sqrt{\delta + 1})$, coinciding with the solution with (−) in Eq. (80).

The non-dimensional Campbell diagrams for the case of long pendulums with $\alpha = 0.1$ and $\delta = 0.2$ are shown in Fig. 7 for two different values of β, namely 1.6 (disc rotor) and 0.2 (long rotor). Such a low value has been used as a limiting case, even though it makes little sense for a

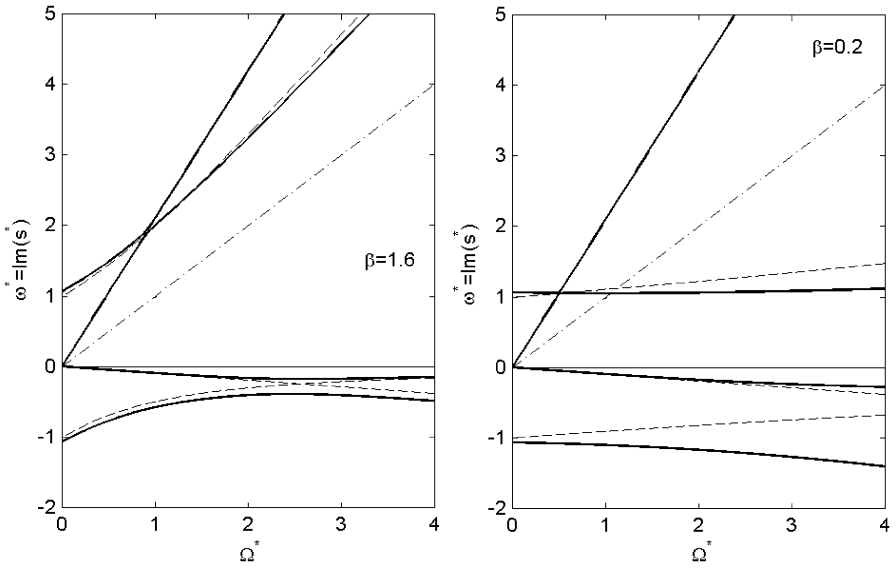

Fig. 7. Campbell diagrams for the case of out-of-plane oscillations of an array of pendulums with $\alpha = 0.1$, $\delta = 0.2$ and $\beta = 1.6$ and $\beta = 0.2$. Note that no field of instability is present. Dashed lines: uncoupled solution; full lines: coupled solution.

rotor with many pendulums. The non-dimensional parameters are the same (except for β) as those used in Fig. 4a.

The decay rate plot is not shown as the real part of s is identical zero: no instability range is present in this case.

While in the case of in-plane oscillations an instability range was found for the case of long pendulums owing to the coupling of the motion of the pendulums and of the supporting disc, no such phenomenon was found for the case of out-of-plane oscillations.

Some numerical results for the complete system, with restoring force and damping, are shown in Fig. 8: the non-dimensional Campbell diagram and the decay rate plot reported deal with the same case in Fig. 7, with $\alpha = 0.1$, $\delta = 0.2$ and two values of β, 1.6 and 0.2. The restoring spring has a stiffness leading to $\omega_p^* = \sqrt{2}$ and the damping parameters are $\zeta_d = 0.05$ and $\zeta_p = 0.1$.

From the figure it is clear that although rotating damping is much higher than non-rotating damping, no field of instability is present.

Also in the case of out-of-plane oscillations rotating damping of the pendulums does not trigger instability. In this case instability cannot be due to the interaction between the motion of the pendulums and of the supports, so that the system is always stable.

2.8. *Dynamics of a row of blades*

As the study of rotating pendulums has shown, the dynamics of an array of blades which may surround a rotor can interact with the dynamics of the rotor as a whole, to the point that instability ranges may occur. In particular, the study of the behaviour of pendulums suggests that in-plane vibrations are more dangerous, from this viewpoint, than out-of-plane vibrations.

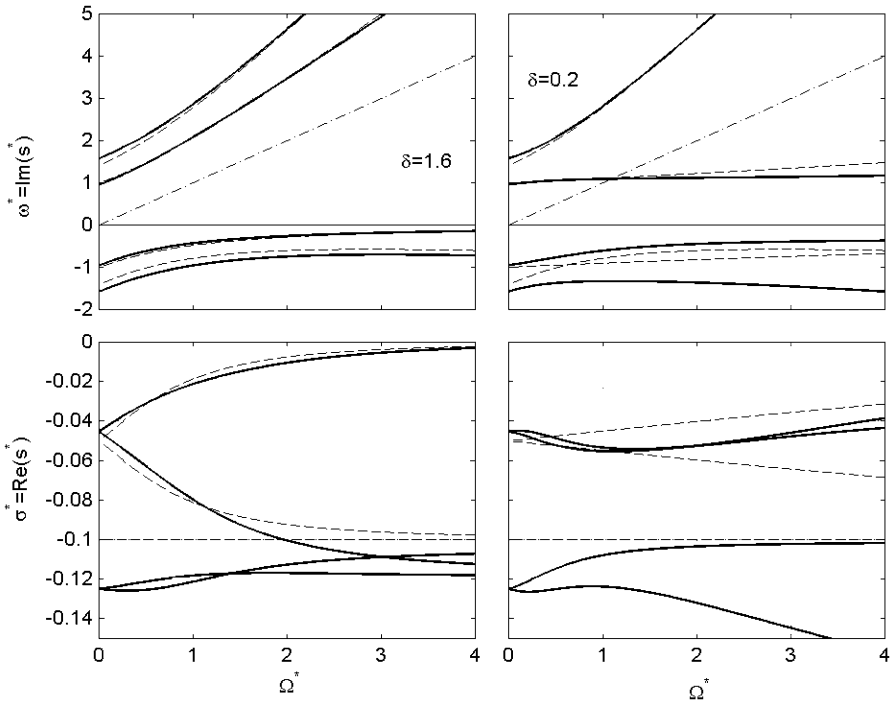

Fig. 8. Campbell diagram and decay rate plot for the out-of-plane oscillations of a row of pendulums with $\alpha = 0.1$, $\delta = 0.2$ and two values of β, 1.6 and 0.2. The other data are $\omega_p^* = \sqrt{2}$, $\zeta_d = 0.05$ and $\zeta_p = 0.1$. Dashed lines: uncoupled solution; full lines: coupled solution.

Unfortunately there is no simple model to substantiate these statements. The present section will be devoted to the construction and the solution of a few highly idealized numerical models, attempting to extract some general rules. These models will be based on the finite element method, using the formulation described in Refs. [8–10]. The dynamics of the array is dealt with in a way which is similar to what has been done for the study of the pendulums. The zeroth order harmonics (like the one shown in Fig. 2a) couples with the torsional and axial dynamics of the shaft, while the first order harmonics (Fig. 2b and c) are coupled with the flexural behaviour. Higher order harmonics do not affect the behaviour of the rotor as a whole, and will not be considered here.

Since the number of parameters is high, no attempt has been done to extract non-dimensional parameters. Consider a system made by a rigid disc, suspended on a spring system, with a number of prismatic blades. The data are summarized in Table 1.

Since the length of the blades is greater than the radius of the disc, they can be defined as *long blades*, to use a term similar to that used for rotating pendulums. In the case of pendulums, this leads to a field of instability.

The model is made by a rigid mass element, a spring element and a row-of 10 blades elements, plus a disc element and two transition elements, since these are required by the code, when blades are present. The uncoupled dynamics are studied in Fig. 9. If the blades are rigid bodies, the behaviour is that of an uncoupled four (real) degrees of freedom system with the inertial

Table 1
Data for the FEM model of a disc with an array of prismatic blades

Disc	Inertial properties m, J_t, J_p	8 kg, 2.6 kg m^2, 4 kg m^2
	Outer radius r_o	100 mm
	Suspension stiffness k_{11}, k_{22} ($k_{12}=0$)	10^7 N/m, 10^7 Nm/rad
Blades	Number n	10
	Square cross-section	10 mm × 10 mm
	Length l	500 mm
Material	E	2.1×10^{11} N/m^2
	ρ	7810 kg/m^3

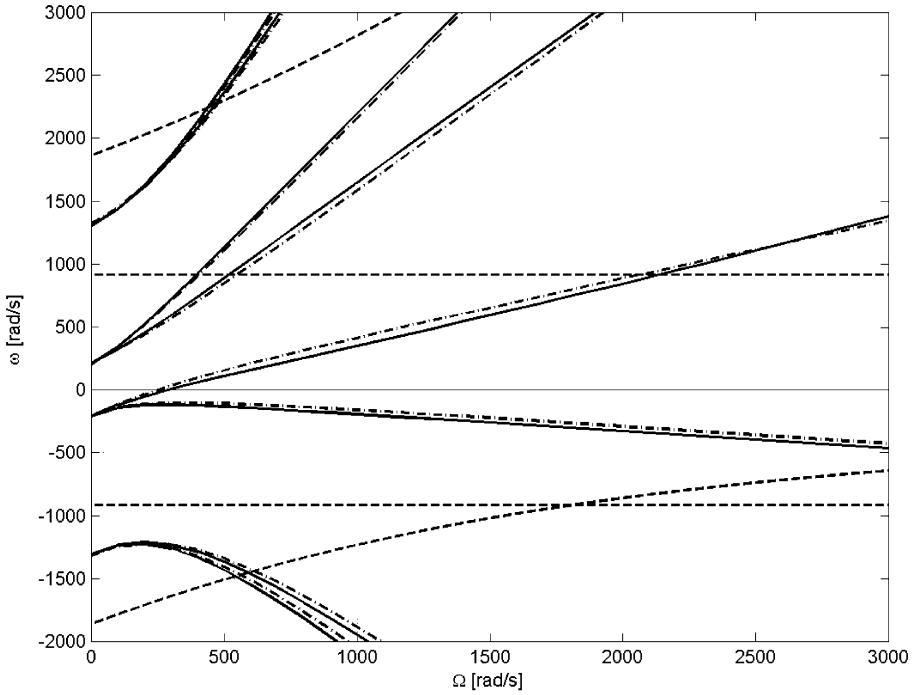

Fig. 9. Uncoupled dynamics of a bladed disc on elastic supports. Full lines: dynamics of the blades on a stiff support; dot and dash curves: same as before but computed through an approximated formula; dashed lines: dynamics of the rigid system on elastic supports.

properties of the whole system, $m=11.92$ kg, $J_{t_T}=2.88$ kg m^2, $J_{p_T}=4.57$ kg m^2. The results are plotted as dashed lines in the Campbell diagram of Fig. 9; owing to uncoupling, the translational modes are those of a Jeffcott rotor.

The full lines in the same figures refer to the dynamics of the flexible blades on a rigid support. Since the cross-section of the blades is square, at standstill the in-plane natural frequencies coincide with the out-of-plane ones. As soon as the spin speed is non-vanishing, however, they differentiate and the curves related to the various modes split in two. The out-of-plane natural frequencies (particularly the first one) increase more sharply with the speed than the in-plane ones.

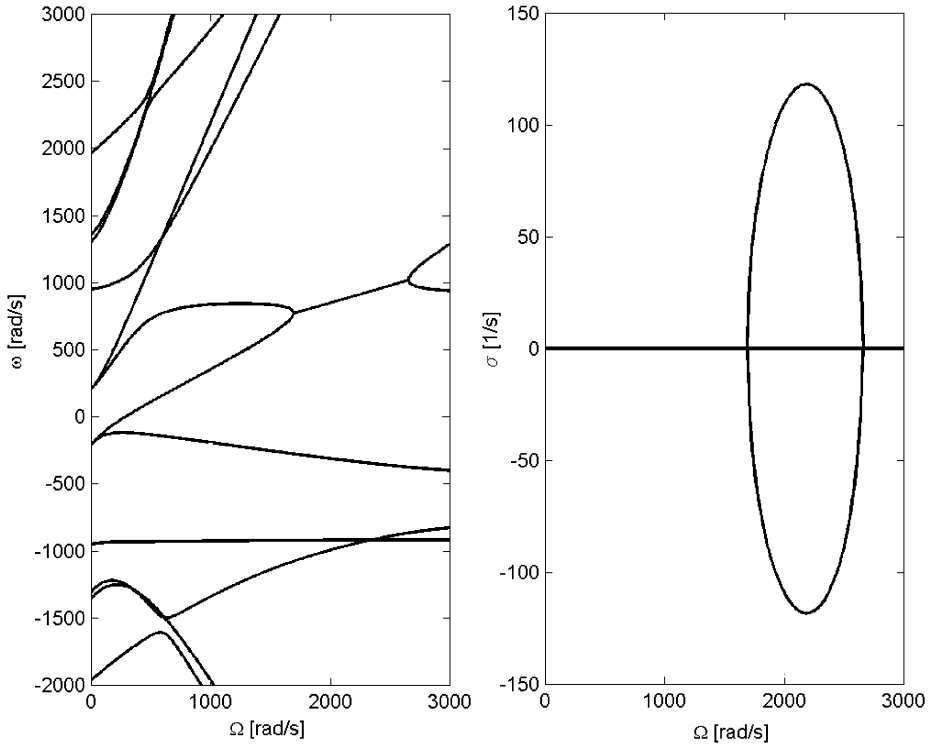

Fig. 10. Coupled dynamics of a bladed disc on elastic supports; Campbell diagram and decay rate plot.

As in the case of long pendulums, the lowest backward mode in the rotating frame becomes a forward mode in the fixed frame. The simplified blade dynamics, computed using the natural frequency at standstill $\omega_{\Omega=0}$ and then using the approximated formula [11]

$$\omega = \sqrt{\omega_{\Omega=0}^2 + \omega_s^2}, \tag{81}$$

where ω_s is the natural frequency of a rotating string of the same mass (to account for centrifugal stiffening), is reported in the same figure with dot-and-dash curves. Note that the results so obtained are remarkably close to those obtained through the FEM.

The coupled dynamics are shown in Fig. 10. The curves related to the disc and blade dynamics interact with each other, and the first backward mode (actually it is backward only in the rotating frame, in the inertial frame it is a forward mode) of the bladed array interacts with the forward translational mode of the rigid system on elastic supports giving way to a field of instability. The latter is very clearly evidenced by the decay rate plot.

Consider now the case of blades with a rectangular cross-section, so that there are no coincident natural frequencies at standstill. The cross-section of the blades in the model was modified, keeping the cross-sectional area constant: a rectangle 2.5 mm × 40 mm is assumed. The dynamic behaviour is then much influenced by the angle the blade makes with the axial direction: if $\psi = 90^\circ$ the blade is aligned along the axial direction (lowest natural frequency is in-plane), while if $\psi = 0$ the blade is perpendicular to the axial direction.

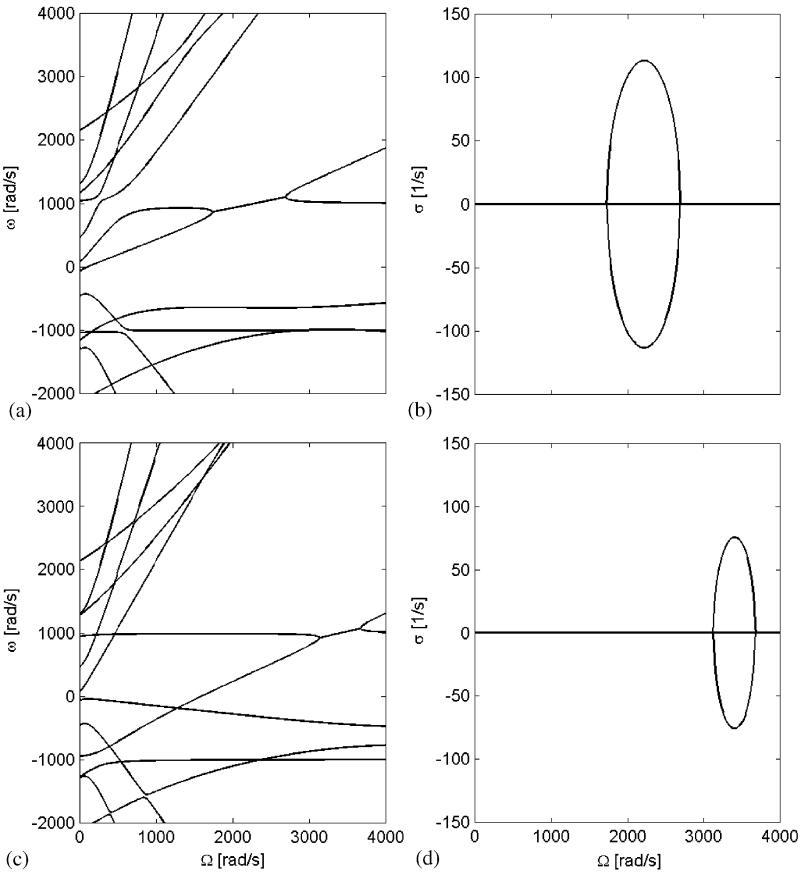

Fig. 11. Bladed disc with blades with rectangular cross-section. Campbell diagram and decay rate plot for the two limiting cases, $\psi = 90^\circ$ (a and b) and $\psi = 0$ (c and d).

The Campbell diagram and the decay rate plot for the two limiting cases, $\psi = 90^\circ$ and $\psi = 0$ are reported in Fig. 11. The instability range shifts towards higher speeds when ψ decreases from 90° (Figs. 11a and b) to 0 (Fig. 11c and d).

The speeds at which the field of instability starts and ends are reported in Fig. 12 as functions of angle ψ.

From the plots of Fig. 11 it is clear that in the case when the cross-section of the blades is aligned with the axial direction, the frequencies of the in-plane modes are lower than those of the out-of-plane ones and the relevant branches in the Campbell diagram do not cross. The opposite occurs when $\psi = 90^\circ$.

To investigate the effect of damping in blades, the same model was modified by assigning a loss factor to the various elements. All rotating elements were given a very high damping ($\eta = 0.1$) while the only non-rotating elements, the springs supporting the system, were given a very low damping ($\eta = 0.005$). The value of the density of the material was lowered to $4000\,\mathrm{kg/m^3}$. The results for the case $\psi = 90^\circ$ are reported in Fig. 13.

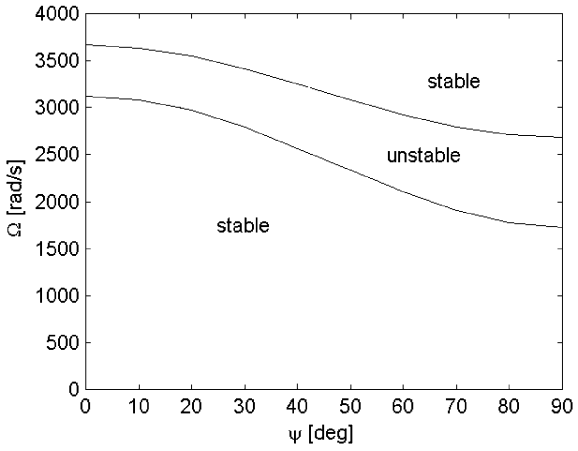

Fig. 12. Bladed disc with blades with rectangular cross-section. Speeds at which the instability range starts and ends as functions of angle ψ.

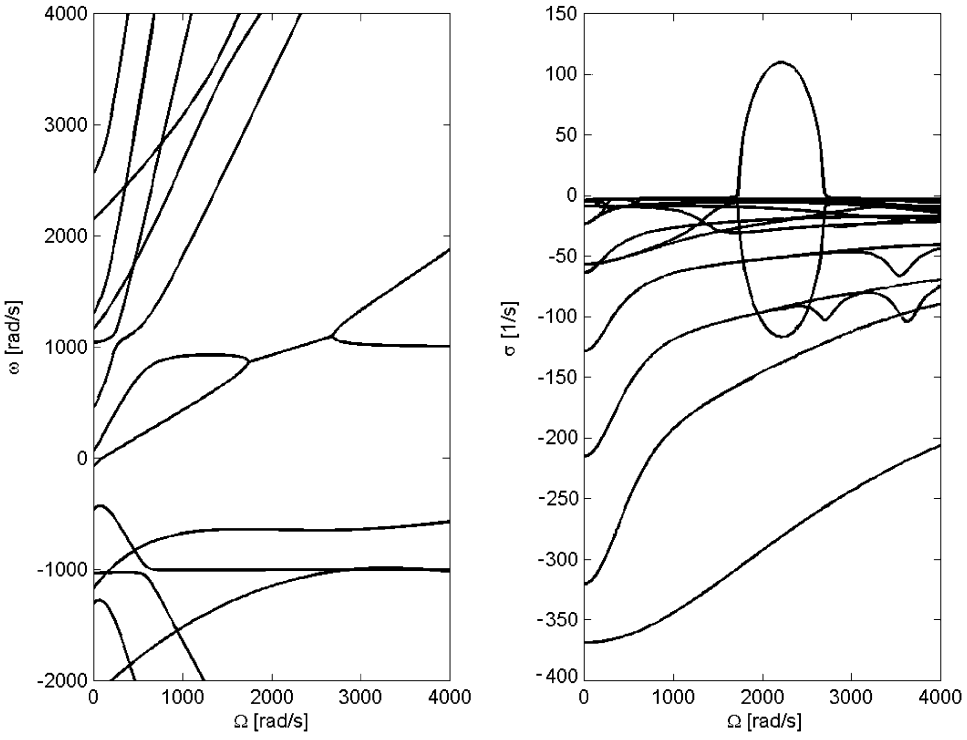

Fig. 13. Campbell diagram and decay rate plot for the bladed disc studied in Fig. 11(a) and (b) ($\psi = 90°$), but with hysteretic damping added. Rotating damping with loss factor $\eta = 0.1$; non-rotating damping with $\eta = 0.005$.

As expected, the effect of damping on the Campbell diagram is not large, while it influences deeply the decay rate plot. In a way which is similar to that which has been seen for the rotating pendulum, the damping associated with the blades does not have an unstabilizing effect,

although it is a form of rotating damping. The instability range is only slightly reduced by the presence of damping, but all blade vibrations have a negative decay rate. The damping associated to the blades, although rotating, does not trigger instability even in the supercritical range.

3. Conclusions

The study of the interaction of the dynamics of a row of rotating pendulums with that of the supporting disc yielded the following conclusions:

- The axial and torsional behaviour of the system are decoupled, and no inertial coupling exists between in-plane and out-of-plane vibrations of the pendulums. This decoupling holds only if the linearized dynamics are considered.
- If the pendulums are *long* (i.e., their length is greater than the radius at which they are attached), an instability range is found where the line related with an in-plane wave which travels backward with respect to the rotor but forward in a fixed frame crosses the line related with the vibration of the supporting disc.
- If the pendulums are short all backward travelling waves also do the same in the fixed frame and no instability range is present.
- Out-of-plane motion never becomes unstable.
- The presence of dampers, either between the disc and the pendulums or between the latter, has no unstabilizing effect. Although rotating, their effect is similar to that of non-rotating dampers.

Some numerical experiments performed on FEM models in which the blades are modelled as prismatic beams essentially confirm the applicability of the results obtained on the pendulums to actual blades.

A question remains: why the damping associated to the blades, although rotating, does not trigger instability even when the rotor works in the supercritical range?

From a mathematical viewpoint, in the solution of the quadratic equation (68) a term $-2j\zeta_p\Omega^*$ under the square root, coming from the square of the coefficient to the term in s^*, cancels with the term $2j\zeta_p\Omega^*$ (typical of rotating damping and usually causing instability) coming from the product of the coefficient of the term in s^{*2} and that in s^{*0} and then no imaginary term remains under the square root. The term $-2j\zeta_p\Omega^*$ is due to an interaction between the gyroscopic (or Coriolis) effect and rotating damping.

This interaction between rotating damping and gyroscopic effect suggests a simple heuristic explanation: the slope on the Campbell diagram of the lines related with blade vibration is higher than that of the bisector of the first quadrant or, in other words, the natural frequencies of the blades increase with the speed in such a way that they work in subcritical conditions even when the rotor as a whole is supercritical. This causes their damping to have no unstabilizing effect, since it works 'locally' in subcritical conditions. This is likely to occur also in other cases, like the vibration of flexible discs or membranes, whose natural frequencies grow quickly with the speed.

Appendix A. Lagrangian and Rayleigh functions

The generalized co-ordinates of the system are $X,\ Y,\ Z,\ \phi_y,\ \phi_X,\ \phi_z,\ \phi_i$, and γ_i $(i = 1, \ldots, n)$; they are all assumed to be small quantities. Since the rotor can perform torsional vibrations, the rotation angle θ is

$$\theta = \Omega t + \phi_z \tag{A.1}$$

and its instant spin speed is

$$\dot{\theta} = \Omega + \dot{\phi}_z. \tag{A.2}$$

The kinetic energy of the rigid body is then [5]

$$\begin{aligned}\mathscr{T}_d = &\tfrac{1}{2} m_d(\dot{X}^2 + \dot{Y}^2 + \dot{Z}^2)\\ &+ \tfrac{1}{2}[J_t(\dot{\phi}_X^2 + \dot{\phi}_y^2) + J_p(\Omega^2 + 2\Omega\dot{\phi}_z + \dot{\phi}_z^2 + 2\Omega\dot{\phi}_X\phi_y)].\end{aligned} \tag{A.3}$$

The potential energy of the springs supporting the rigid body is

$$\begin{aligned}\mathscr{U}_d = &\frac{1}{2}\begin{Bmatrix} X \\ \phi_y \end{Bmatrix}^{\mathrm{T}} \begin{bmatrix} k_{11} & k_{12} \\ k_{12} & k_{22} \end{bmatrix} \begin{Bmatrix} X \\ \phi_y \end{Bmatrix}\\ &+ \frac{1}{2}\begin{Bmatrix} Y \\ \phi_X \end{Bmatrix}^{\mathrm{T}} \begin{bmatrix} k_{11} & -k_{12} \\ -k_{12} & k_{22} \end{bmatrix} \begin{Bmatrix} Y \\ \phi_x \end{Bmatrix} + \tfrac{1}{2} k_a Z^2 + \tfrac{1}{2} k_t \phi_z^2,\end{aligned} \tag{A.4}$$

i.e. ,

$$\begin{aligned}\mathscr{U}_d = &\tfrac{1}{2} k_{11}(X^2 + Y^2) + \tfrac{1}{2} k_{22}(\phi_X^2 + \phi_y^2) + k_{12}(X\phi_y - Y\phi_X)\\ &+ \tfrac{1}{2} k_a Z^2 + \tfrac{1}{2} k_t \phi_z^2.\end{aligned} \tag{A.5}$$

In a similar way, the Rayleigh dissipative function of the suspension system is

$$\begin{aligned}\mathscr{F}_d = &\tfrac{1}{2} c_{11}(\dot{X}^2 + \dot{Y}^2) + \tfrac{1}{2} c_{22}(\dot{\phi}_X^2 + \dot{\phi}_y^2) + c_{12}(\dot{X}\dot{\phi}_y - \dot{Y}\dot{\phi}_X) + \tfrac{1}{2} c_a \dot{Z}^2\\ &+ \tfrac{1}{2} c_t \dot{\phi}_z^2.\end{aligned} \tag{A.6}$$

The position in xy plane of point P_i in which the bob of the ith pendulum is located is

$$(\overline{P_i - O}) = \begin{Bmatrix} X \\ Y \\ Z \end{Bmatrix} + \mathbf{R}_1^{\mathrm{T}}\mathbf{R}_2^{\mathrm{T}}\mathbf{R}_3^{\mathrm{T}} \begin{Bmatrix} r + l\cos(\phi_i)\cos(\gamma_i) \\ l\sin(\phi_i)\cos(\gamma_i) \\ l\sin(\gamma_i) \end{Bmatrix}, \tag{A.7}$$

where matrices $\mathbf{R}_1$, $\mathbf{R}_2$ and $\mathbf{R}_3$ are defined in Section 4.4.1 in [5] and angle θ_i included in matrix $\mathbf{R}_3$ is

$$\theta_i = \Omega t + \phi_z + \psi_i \tag{A.8}$$

and ψ_i is the angle which defines the position of the ith pendulum in the row

$$\psi_i = 2\pi \frac{(i-1)}{n}. \tag{A.9}$$

Since the latter is a constant, $\dot{\theta}_i = \Omega + \dot{\phi}_z = \dot{\theta}$ and $\ddot{\theta}_i = \ddot{\phi}_z = \ddot{\theta}$. They are the same for all pendulums.

By differentiating the expression of the position of point P_i with respect to time the velocity and then the kinetic energy of the ith pendulum can be obtained. The complete expression is too complicated to be reported here. When taking into account the small displacements assumptions, by neglecting all powers of small quantities following the second one, it reduces to

$$\begin{aligned}\mathscr{T}_i = {} & \tfrac{1}{2} m\{\dot{X}^2 + \dot{Y}^2 + \dot{Z}^2 + \dot{\phi}_i^2 l^2 + \dot{\gamma}_i^2 l^2 + 2\dot{Z}\dot{\gamma}_i l - \dot{\theta}^2 \phi_i^2 r l \\ & + (\dot{\theta}^2 + 2\dot{\phi}_X \dot{\theta}\phi_y)(r+l)^2 + (2\dot{\phi}_i \dot{\theta} - \dot{\theta}^2 \gamma_i^2) l(l+r) \\ & + 2[(-\dot{\phi}_y \gamma \dot{\theta} l - \dot{\theta}\dot{X} + \dot{Z}\dot{\phi}_X + \dot{\phi}_X \dot{\gamma}_i l + \dot{Z}\dot{\theta}\phi_y)(l+r) \\ & - \dot{X}\dot{\phi}_i l - \dot{\theta}\dot{Y}\phi_i l] \sin(\theta_i) + 2[(-\dot{\gamma}_i \dot{\phi}_y l + \dot{\theta}\dot{Y} + \dot{Z}\dot{\theta}\phi_X - \dot{Z}\dot{\phi}_y \\ & - \dot{\theta}\dot{\phi}_X \gamma_i l)(r+l) + \dot{\phi}_i \dot{Y} l - \dot{\theta}\dot{X}\phi_i l] \cos(\theta_i) + \dot{\phi}_y^2 (r+l)^2 \cos^2(\theta_i) \\ & + \dot{\phi}_X^2 (r+l)^2 \sin^2(\theta_i) - 2\dot{\phi}_y \dot{\phi}_X (l+r)^2 \cos(\theta_i) \sin(\theta_i)\}. \end{aligned} \tag{A.10}$$

The potential energy of the spring and the Rayleigh dissipative function of the dampers of the ith pendulum are

$$\mathscr{U}_{P_i} = \tfrac{1}{2} k_p (\phi_i^2 + \gamma_i^2), \tag{A.11}$$

$$\mathscr{F}_{P_i} = \tfrac{1}{2} l^2 c_p (\dot{\phi}_i^2 + \dot{\gamma}_i^2) + \tfrac{1}{2} l^2 c_q [(\dot{\phi}_i - \dot{\phi}_{i+1})^2 + (\dot{\gamma}_i + \dot{\gamma}_{i+1})^2], \tag{A.12}$$

where $\dot{\phi}_{n+1} = \dot{\phi}_1$ and $\dot{\gamma}_{n+1} = \dot{\gamma}_1$.

The Lagrangian and the Rayleigh functions of the system are then

$$\mathscr{L} = \mathscr{T}_d - \mathscr{U}_d + \sum_{i=1}^{n} (\mathscr{T}_{P_i} - \mathscr{U}_{P_i}), \tag{A.13}$$

$$\mathscr{F} = \mathscr{F}_d + \sum_{i=1}^{n} \mathscr{F}_{P_i}. \tag{A.14}$$

Appendix B. Nomenclature

c_a	axial damping coefficient
c_p	damping coefficient of the pendulums

c_q damping coefficient of the dampers between the pendulums
c_t torsional damping coefficient
j imaginary unit ($j = \sqrt{-1}$)
l length of the pendulums
m mass of each pendulum
m_d mass of the rigid body
m_t total mass
n number of pendulums
r radius
k_a axial stiffness
k_t torsional stiffness
$\mathbf{C}$ damping matrix
$\mathscr{F}$ rayleigh dissipation function
J_p polar moment of inertia
J_t transversal moment of inertia
$\mathbf{K}$ stiffness matrix
$\mathscr{L}$ lagrangian function
$\mathscr{T}$ kinetic energy
$\mathscr{U}$ potential energy
α_i non-dimensional coefficient
β ratio J_p/J_t
δ ratio r/l
γ_i out-of-plane angle of pendulums
ζ damping ratio
ϕ_i in-of-plane angle of pendulums
ϕ_X rotation about X-axis
ϕ_y rotation about y-axis
ϕ_z torsional rotation
ψ_i angles defining the positions of pendulums
ω_{ax} axial natural frequency
ω_{ip} in-plane natural frequency
ω_l lateral natural frequency
ω_{op} out-of-plane natural frequency
ω_{tors} torsional natural frequency
$\Delta\psi$ angle between pendulums ($\Delta\psi = 2\pi/n$)
Ω rotational speed

References

[1] S.H. Crandall, J. Dugundji, Resonant whirling of aircraft propeller-engine systems, *Journal of Applied Mechanics* 48 (1981) 929–935.
[2] S.H. Crandall, Rotordynamics, in: W. Kliemann, N. Sri Namachchivaya (Eds.), *Nonlinear Dynamics and Stochastic Mechanics*, CRC Press, Boca Raton, FL, 1995.
[3] J.P. Den Hartog, *Mechanical Vibrations*, McGraw-Hill, New York, 1934.

[4] M. Dimentberg, *Flexural Vibrations of Rotating Shafts*, Butterworth, London, England, 1961.
[5] G. Genta, *Vibration of Structures and Machines*, 3rd Edition, Springer, New York, 1998.
[6] A. Muszinska, Whirl and whip-rotor/bearing stability problems, *Journal of Sound and Vibration* 110 (3) (1986) 443–462.
[7] S.H. Crandall, J.W. Mroszczyk, Conservative and nonconservative coupling in dynamic systems, *Proceedings International Conference on Vibrations in Rotating Machinery*, Institute of Mechanical Engineering Conference Publications, Vol. 7, Institute of Mechanical Engineers, London, 1988, pp. 567–572.
[8] G. Genta, A. Tonoli, A harmonic finite element for the analysis of flexural, torsional and axial rotordynamic behavior of discs, *Journal of Sound and Vibration* 196 (1) (1996) 19–43.
[9] G. Genta, A. Tonoli, A harmonic finite element for the analysis of flexural, torsional and axial rotordynamic behavior of bladed arrays, *Journal of Sound and Vibration* 207 (5) (1997) 693–720.
[10] G. Genta, D. Bassani, C. Delprete, DYNROT: a finite element code for rotordynamic analysis based on complex co-ordinates, *Engineering Computations* 13 (6) (1966) 86–99.
[11] H. Lamb, R.V. Southwell, The vibrations of a spinning disk, *Proceedings of the Royal Society of London* 99 (1921) 272–280.